Revision 1

The replacement of chalcopyrite by bornite under hydrothermal conditions

Jing Zhao[1,2], Joël Brugger[1,3], Yung Ngothai[2], and Allan Pring[1,4*]

[1]Department of Mineralogy, South Australian Museum, North Terrace, Adelaide, SA 5000, Australia

[2]School of Chemical Engineering, University of Adelaide, Adelaide, SA 5005, Australia

[3]School of Geosciences, Monash University, Clayton, VIC 3800, Australia

[4]School of Chemical and Physical Sciences, Flinders University, Bedford Park, SA 5042, Australia

*Corresponding author: allan.pring@samuseum.sa.gov.au

Abstract

We report the replacement of chalcopyrite by bornite under hydrothermal conditions in solutions containing Cu(I) and hydrosulfide over the temperature range 200-320 °C at autogenous pressures. Chalcopyrite was replaced by bornite under all studied conditions. The reaction proceeds via an interface coupled dissolution-reprecipitation (ICDR) mechanism and via additional overgrowth of bornite from the bulk solution. Initially, the reaction is fast and results in a bornite rim of homogeneous thickness. Reaction rates then slow down, probably reflecting healing of the porosity, and the reaction proceeds predominantly along twin boundaries of the chalcopyrite.

The composition of the bornite product is generally Cu-rich, corresponding to the bornite (Cu_5FeS_4; Bn) - digenite (Cu_9S_5; Dg) solid solution (*bdss*). The Cu and Fe contents were controlled principally by temperature, with solution pH having only a small effect. The percentage of Cu in *bdss* decreased and the percentage of Fe increased with increasing reaction temperature: at 200 ˚C a composition of $Bn_{47}Dg_{53}$ was obtained; at 300 ˚C the composition was $Bn_{90}Dg_{10}$ and at 320 ˚C it was near-stoichiometric bornite. The influence of temperature rather than solution chemistry on the composition of *bdss*, as well as the homogeneity of the bornite product grown both via replacement of chalcopyrite and from the bulk solution as overgrowth, are interpreted to reflect buffering of the bornite activity in *bdss* via solids (e.g., reaction chalcopyrite + 2 chalcocite = bornite).

Only the end-member compositions of the *bdss* are found in nature, indicating that the products obtained are metastable, and illustrating the importance of reaction mechanism for controlling the chemistry of the mineral product. The unique features of the chalcopyrite to bornite reaction investigated here are related to interaction between a solution controlled ICDR reaction with solid-state diffusion processes driving porosity healing.

Keywords: chalcopyrite, bornite, mineral replacement reaction, diffusion, hydrothermal, bornite-digenite solid solution.

Introduction

Chalcopyrite ($CuFeS_2$) and bornite (Cu_5FeS_4) are the most abundant primary Cu-bearing sulfides across a wide range of ore deposit types. In nature the textures of some chalcopyrite-bornite assemblages can be interpreted in terms of solid-state exsolution or unmixing processes, e.g. bornite intergrown with a maze of minute chalcopyrite needles (Ramdohr 1980; Cook et al. 2011). The majority of chalcopyrite and bornite intergrowths, however, show textures consistent with fluid-mediated replacement reactions. The replacement of chalcopyrite by bornite is common in sulfide chimneys from active seafloor hot springs (e.g., Graham et al. 1988; Haymon 1983; Tivey 1995); further replacement of chalcopyrite by bornite also happens during weathering of such massive sulfide deposits (Halbach et al. 1998). Oszczepalski (1999) showed that chalcopyrite was preferentially replaced by bornite, which could in turn be replaced by Cu-sulfides such as chalcocite, covellite and digenite in Kupferschiefer ores from Poland. Indeed, chalcopyrite-bornite intergrowths found in many primary copper sulfide ores are believed to have formed either by bornite replacing chalcopyrite or vice versa (Ramdohr 1980; Robb 2005).

The transformation mechanism of chalcopyrite and bornite intergrowths has been the subject of only a small number of experimental studies either under solid-state or low temperature hydrothermal conditions. Amcoff (1988) undertook a detailed study on the solid-state replacement of chalcopyrite by bornite between 200 and 500 °C, showing that chalcopyrite reacted with chalcocite to form bornite under relatively

reducing conditions. The reaction is claimed to be structurally controlled by the inter-diffusions of Fe and Cu in the S lattices. Roberts (1963) conducted a series of experiments to investigate the transformation of chalcopyrite into bornite in Cu-sulfate aqueous solutions at low temperature (<150 °C), showing that chalcopyrite could be converted to bornite after six days at 100 °C, and that the product bornite could be converted back to chalcopyrite by adding an excess of sulfide and ferrous ions under the same conditions.

Based on previous studies of mineral replacement reactions in a range of important sulfide minerals including pyrite (Qian et al. 2010, 2011, 2013), violarite (Tenailleau et al. 2006; Xia et al. 2009a; Brugger et al. 2010) and marcasite (Qian et al. 2011), we recently undertook an experimental study of the formation of chalcopyrite and bornite via the sulfidation of hematite under hydrothermal conditions, more specifically the replacement of hematite by chalcopyrite and bornite upon reaction with Cu-S-rich fluids in the temperature interval 200 to 300 °C (Zhao et al. 2014). This study showed that hematite was replaced by chalcopyrite under all studied conditions and the chalcopyrite product could further react with Cu and S in the solution to form bornite. The replacement of chalcopyrite by bornite was only observed on the outer surface of chalcopyrite and no bornite was observed at the reaction front between hematite and chalcopyrite. The overall reaction of chalcopyrite replacement by bornite can be written as (assuming conservation of Fe, basic pH; Zhao et al. 2014):

$$CuFeS_2(s) + 4Cu(HS)_2^- + 2OH^- = Cu_5FeS_4(s) + 6HS^- + 2H_2O;\ \Delta V\sim 226\% \quad (1)$$

Note that reaction (1) is associated with a large volume increase.

Here, we report the results of an experimental study of reaction (1) under hydrothermal conditions at temperatures up to 320 °C. The aim was to determine the reaction texture, the composition and homogeneity of the product, and the mechanism of the replacement of chalcopyrite by bornite, by exploring the formation of bornite over a range of physical and chemical conditions. Above 265 °C, bornite (Cu_5FeS_4) and digenite (Cu_9S_5) form a complete solid solution, the bornite-digenite solid solution (*bdss*), and in this paper we will refer in general terms to compositions in the bornite-digenite solid solution (*bdss*) as bornite or *bdss*. When discussing specific compositions in the solid solution series we will denote them by their bornite and digenite factions, calculated on the basis of the stoichiometric Cu content (Bn_xDg_{1-x}).

Samples and methods

Preparation of starting samples and thermodynamic calculations

Chalcopyrite from the Wallaroo Mines, South Australian (SA Museum sample G22621) was used as starting material throughout this study. The purity of chalcopyrite was established using powder X-ray diffraction and electron probe microanalysis. The average composition of chalcopyrite is $Cu_{1.04(8)}Fe_{1.05(2)}S_{1.91(4)}$ (mean of 24 analyses). Chalcopyrite was crushed and fragments were washed in an ultrasonic bath, and carefully sieved into a 125 to 150 µm size fraction. All other chemical reagents including buffer solutions were analytical grade reagents. The buffer solutions were prepared as described in Zhao et al. (2014), and their compositions (total concentrations ~1 mole•kg^{-1}) are given in Table 1. The $pH_{25°C}$ values shown in Table 1 were measured at room temperature, and the pH_T values at reaction temperatures listed in Tables 2 and 3 were calculated using the HCh geochemical modeling software (Shvarov and Bastrakov 1999). The calculations were

119 performed considering all the ingredient in each run, including the compositions of
120 buffer solutions and the added amounts of NaCl, chalcopyrite, CuCl and
121 thioacetamide. For example for the CB10 solution, the calculation was made for 5 g
122 H_2O, 0.01 g chalcopyrite, 0.0215 g CuCl, 0.002245 mole NaOH, 0.0026650 mole
123 H_3BO_3, 0.005 mole NaCl and 0.00252 mole NH_3+H_2S. Reaction extent (i.e., models
124 with and without bornite) had little effect on the calculated pH (<0.01 pH unit), while
125 removing Cu/Fe from the model resulted in differences of <0.2 pH units on the
126 calculated pH_T. The accuracy of the calculated pH_T is limited both by the complexity
127 of the chemical system under consideration and by the quality of thermodynamic
128 properties, and the values should be considered as indicative only. Overall, the
129 calculations suggest that the different buffers result in pH varying for acidic to near-
130 neutral and basic at the experimental temperatures. Thermodynamic data were taken
131 from the UNITHERM database (Shvarov and Bastrakov 1999), except for Cu(I)-Cl
132 (Liu and McPhail 2005; Brugger et al. 2007; Mei et al. 2014), Cu(I)-HS (Akinfiev and
133 Zotov 2001) and Fe(II)-Cl complexes (Testemale et al. 2009). The following Fe, Cu
134 and S aqueous species were included in the model: Fe^{2+}; $FeOH^+$; $Fe(OH)_2$(aq);
135 $Fe(OH)_3^-$; $FeCl^+$; $FeSO_4$(aq); Fe^{3+}; $FeOH^{2+}$; $Fe(OH)_2^+$; $Fe(OH)_3$; $Fe(OH)_4^-$; $FeCl^{2+}$;
136 $FeCl_2^+$; $FeCl_2$; $FeCl_4^{2-}$; Cu^+; CuOH(aq); $Cu(OH)_2^-$; CuCl; $CuCl_2^-$; $CuCl_3^{2-}$; CuHS(aq);
137 $Cu(HS)_2^-$; Cu^{2+}; $CuOH^+$; $Cu(OH)_2$; $Cu(OH)_3^-$; $Cu(OH)_4^{2-}$; $CuCl^+$; $CuCl_2$(aq); $CuCl_3^-$;
138 $CuCl_4^{2-}$; $NaCuCl_2$(aq); S_2^{2-}; HS^-; H_2S; $S_2O_3^{2-}$; $HS_2O_3^-$; $H_2S_2O_3$(aq); SO_2(aq); SO_3^{2-};
139 HSO_3^-; SO_4^{2-}; HSO_4^-; NaHS(aq).

140 **Hydrothermal experiments**

141 The experiments were conducted with excess sulfide and with the amounts of Cu (as
142 CuCl(s)) required to convert all chalcopyrite to bornite. In each run, 10 mg of
143 chalcopyrite crystal fragments (55 µmoles), 21.5 mg CuCl(s) (217 µmoles), 0.1890 g

144 thioacetamide (liberating ~0.5 mole•kg^{-1} S into solution) and 5 mL reaction solution
145 were carefully measured and added into an 8 mL titanium autoclave in an argon-filed
146 anoxic glove box. Thioacetamide was used as a source of reduced sulfur.
147 Thioacetamide was added as a poorly soluble solid at room temperature;
148 thioacetamide breaks down rapidly above 100 °C, liberating H_2S (Qian et al. 2011).
149
150 The sealed cells were left in electric Muffle furnaces (with a temperature regulation
151 precision of 2 °C) at a constant temperature over the duration of the experiments. At
152 the end of the runs, the autoclaves were quenched to room temperature in a large
153 volume of cold water (~10 L) for 20 minutes. The solids were rinsed three times using
154 Milli-Q water followed by acetone. Results from leaking runs were not considered in
155 this study. During the experiments, the pressures in the autoclaves were autogenous
156 pressures (~108 bar for a 1 mole•kg^{-1} NaCl solution; Bischoff 1991). To investigate
157 the effects of pH and temperature on the reaction rate and the composition of bornite,
158 experiments were undertaken in CP2, CA4, CP7 and CB10 buffer solutions (Table 1)
159 at temperatures ranging from 200 to 320 °C.

160 **Analysis methodology**

161 The extent of the transformation was determined by Rietveld quantitative phase
162 analysis (QPA) of powder X-ray diffraction data with the program Topas (Bruker
163 AXS 2009), using diffraction data in the 2θ range from 4 to 100° (Co $K\alpha_1$radiation).
164 Details of sample preparation and measurements are given in Zhao et al. (2009, 2013).
165 A Pseudo-Voigt function and 6th order Chebychev polynomial were used to model the
166 peak shapes and the background, respectively. For each diffractogram, the zero shift
167 and scale factors for chalcopyrite (ICSD database #94554), bornite (#200424, a =
168 10.981 Å) and a bornite-digenite phase (#42709) with cubic symmetry and a cell

repeat of 5.56 Å, which corresponds to a simple cubic subcell of the bornite-digenite solid solution (Vaughan and Craig 1978), were refined. The occurrence of two bdss phases is most likely due to the breakdown of the solid solution during gridding (Grguric et al. 1999), because it only appears in some patterns and not systematically with reaction temperature. The reaction extents (y) were calculated from the Rietveld refinement results as $y = 1-y_t$, where y_t is weight percentage of chalcopyrite at time t. For reactions undertaken at temperatures below 250 °C, it was not possible to use QPA methods as the bornite reflections in the x-ray patterns were very broad and relatively weak, indicative of a fine grained product and a low extent of reaction.

The characterization of the morphological and textural features of the reacted grains was undertaken using a Philips XL30 field emission scanning electron microscope (FESEM) at Adelaide Microscopy, University of Adelaide. The chemical compositions of the products were determined using a Cameca SX-51 electron probe microanalysis (EPMA) at Adelaide Microscopy, University of Adelaide.

Results

The replacement of chalcopyrite by bornite

XRD analysis shows that chalcopyrite was replaced by bornite under all the conditions explored in this study. The reaction extents for experiments conducted at 300 °C using buffer solution CB10 show an initial fast replacement rate (Runs C8-C16, Table 2). For example, 32±5 wt% of chalcopyrite was replaced by bornite (Run C9) after 6 hr reaction, and the extent increased to 77±5 wt% after 24 hr reaction (Run C11), and then remained near this value over the next 48 hr. After ≥120 hr of total reaction time, most of the chalcopyrite had been replaced (≥ 90 wt% bornite).

Under the SEM, the original chalcopyrite gains are characterized by sharp edges and smooth conchoidal surfaces (Fig. 1a). After 72 hr reaction in buffer solution CB10 at 300 °C (Run C13), they consist of compound particles cemented together by a layer of bornite (Fig. 1b). On the outside of the grains, the newly formed bornite consists of microcrystals ranging in size up to 2 µm across (Fig. 1c). Particle cementation and idiomorphic bornite crystals both indicate that some bornite grew out of the solution rather than via chalcopyrite replacement. Back-scattered electron images of cross sections of partially reacted grains show a homogeneous bornite layer surrounding a chalcopyrite core (Fig. 2a). The replacement reaction initiates at the outer surface of the original chalcopyrite grain and also progresses along cracks within the chalcopyrite grains (Fig. 2c). As the reaction extent increases, many grains show herringbone textures, which suggest preferential replacement of chalcopyrite along the {011} direction corresponding to the compositional plane for chalcopyrite twinning (Fig. 2b). The reaction interface between chalcopyrite and bornite presents a sharp boundary (Fig. 2d), and the replacing bornite shows porosity, with coarser porosity on the outside of the bornite layer (Fig. 2e) and the finer porosity (< 200 nm) near the reaction interface (Fig. 2d). The bornite with the coarser porosity formed via overgrowth rather than chalcopyrite replacement. Note that in these back-scattered images that there is no evidence of chemical zoning or exsolution of digenite within the bornite rims. Similarly, electron microprobe data suggest that the composition of the bornite rims are homogeneous for reaction temperatures above 200 °C (Table 3).

Also of note is that, as reported in Zhao et al. (2014), a black suspension of Cu_2S (chalcocite) was observed after opening the autoclaves for reaction extent of ~25% or

less, due to the reaction of Cu(I) and H_2S and the relatively low solubility of Cu(I) in S-bearing fluids at our experimental temperatures. The black solution is absent at higher reaction extents because excess Cu is consumed by the formation of bornite.

Controls on the rate of transformation

Experimental runs undertaken over a range of temperatures and pHs show that the *reaction rates* vary depending on both reaction temperatures (T4-T7) and solution pH (Runs C5-C7 and C11). Specifically, the replacement reaction is favored by higher temperature and near-neutral to basic pH_T. After 24 hour reaction time, the greatest reaction extent occurred in buffer solution CB10 at 300 ˚C (Run C11), showing 77±5% replacement, compared to only 16±5% at 250 ˚C (Run C4; Fig. 3). The lowest extent of transformation was associated with the CP2 buffer solution, where only ~3% replacement was obtained at 250 ˚C (Run C1) and 27±5% at 300 ˚C (Run C5). The reaction extent for runs using buffer solution CA4 increased from 5% at 250 ˚C (Run C2) to 33±5% at 300 ˚C (Run C6), and using buffer solution CP7 increased from 15±5% at 250 ˚C (Run C3) to 72±5% at 300 ˚C (Run C6).

The hydrolysis rate of thioacetamide to form HS^-/H_2S(aq) is fast compared to the rates of these replacement reactions over the temperature range (Qian et al. 2011), and the above results truly reflect the effect of temperature and pH on the replacement reaction rate.

Controls on the composition of the products

Electron microprobe analyses showed that the composition of the bornite rims around the chalcopyrite is homogeneous within individual grains, i.e. the composition at the bornite that formed via overgrowth is the same as that forming via replacement of chalcopyrite. Bornite compositions are related to reaction temperature. Experiments

carried out in solution CB10 at temperatures ranging from 200 to 320 ˚C illustrate that the bulk bornite compositions become more Cu-rich as temperature decreases (Table 3; Fig. 5a), while the percentage of Fe increased with increasing reaction temperature (Fig. 5b). The composition of bornite at 320 ˚C is $Cu_{5.16(9)}Fe_{0.86(7)}S_{4.00}$, which is almost stoichiometric bornite. As the reaction temperature decreases to 300 ˚C, the percentage of Cu in bornite increases and the composition of bornite is $Cu_{5.23(6)}Fe_{0.81(6)}S_{4.00}$, which is related to the bornite-digenite solid solution (*bdss*) of $Bn_{90}Dg_{10}$. The compositions of bornite at 260 ˚C and 240 ˚C are $Cu_{5.81(9)}Fe_{0.60(8)}S_{4.00}$ and $Cu_{6.04(7)}Fe_{0.45(9)}S_{4.00}$, which correspond to $Bn_{63}Dg_{37}$ and $Bn_{53}Dg_{47}$, respectively. Experimental runs undertaken over a range of pHs show that the composition of bornite did not vary significantly with pH (Table 3; Figs. 5a and 5b). At 300 ˚C, the compositions of bornite in runs C5 ($pH_T = 3.75$; $Cu_{5.21(6)}Fe_{0.85(4)}S_{4.00}$), C6 ($pH_T = 4.39$; $Cu_{5.20(9)}Fe_{0.85(5)}S_{4.00}$), and C10 ($pH_T = 7.43$; $Cu_{5.23(6)}Fe_{0.81(6)}S_{4.00}$) are effectively identical. At 250 ˚C, the composition of bornite varies from $Cu_{6.03(8)}Fe_{0.59(8)}S_{4.00}$ to $Cu_{6.30(7)}Fe_{0.50(6)}S_{4.00}$, which is a narrow range in comparison of the effect of temperature.

Discussion

Reaction mechanism and kinetics

The replacement of chalcopyrite by bornite under hydrothermal conditions is characterized by a sharp reaction front between chalcopyrite and bornite, with no visible gap at the reaction front. The reaction starts at the surface of the chalcopyrite grains or along cracks within the chalcopyrite and proceeds towards the crystal core (Fig. 2). These textural characteristics indicate that bornite immediately precipitated as chalcopyrite dissolved, i.e. chalcopyrite dissolution was the rate-limiting step rather

than bornite precipitation (Xia et al. 2009a). Hence, the replacement of chalcopyrite by bornite is an example of an interface coupled dissolution-reprecipitation (ICDR) reaction (Putnis 2009). In the cases where the bulk volume change of the reaction is small, such as the transformation of pentlandite to violarite under mild hydrothermal conditions (Tenailleau et al. 2006; Xia et al. 2009a), the dissolution of the parent phase is spatially tightly coupled with the precipitation of the product phase at the reaction front, resulting in pseudomorphic preservation of grain shape and textural features. However, ICDR reactions with large volume increase, such as the replacement of hematite by chalcopyrite (Zhao et al. 2014), includes not only the replacement at the reaction front but also the overgrowth of product on the outside of grains. The volume changes associated with the overall replacement of chalcopyrite by bornite is of the order of 226% based on the conservation of Fe (equation (1)). Fe conservation is the most likely assumption, given the low Fe solubility in S-rich solutions (Fig. 5c) and the absence of Fe-phases apart from chalcopyrite and bornite. Chalcopyrite and bornite are part of the same broad (zinc blende-antifluorite) structural family, consisting of a cubic close-packed array of S atoms with metal cations occupying available tetrahedral sites in the S lattice. If the volume change is calculated on the basis of the preservation of the S lattice, which is common to both chalcopyrite and bornite, then the volume increase is only 13% (reaction (2)).

$$2CuFeS_2(s) + 3Cu(HS)_2^- + 3OH^- = Cu_5FeS_4(s) + Fe(OH)_2(aq) + 6HS^- + 0.5H_2O + 0.25O_2(g);\ \Delta V\sim 13\% \quad \text{(lattice S conservation)} \quad (2)$$

The aqueous species used for writing Reaction (2) are the predicted predominant species in buffer CB10 at 300 ˚C. Note that Fe(II) and Cu(I) are the most stable oxidation states of Fe and Cu in solution under the conditions used in our experiments

(Etschmann et al. 2010; Testemale et al. 2009). In detail, the factors that control ICDR reactions are complex and ultimately governed by the interplay between the relative kinetics of the reductive dissolution of chalcopyrite (reaction 3) and the oxidative precipitation of bornite (reaction 4):

$$CuFeS_2(s) + OH^- + 1.5H_2O = Cu(HS)_2^- + Fe(OH)_2(aq) + 0.75O_2(aq) \quad (3)$$

$$5Cu(HS)_2^- + Fe(OH)_2(aq) + OH^- + 0.25O_2(aq) = Cu_5FeS_4(s) + 6HS^- + 3.5\ H_2O. \quad (4)$$

Preserving the S lattice during the replacement requires the loss of 2 of the 4 Fe atoms in the chalcopyrite subcell to solution at the reaction interface and the addition of 8 Cu atoms per subcell from the solution. About half of the aqueous Fe generated at the reaction front must be transported to the bulk solution through the pores/cracks in the product bornite, and the excess of aqueous Fe causes the formation of bornite overgrowth at the outer layer of bornite, via a reaction such as (4). Hence, the overgrowth of bornite indicates the capacity of Fe to move through the newly formed bornite to react with excess Cu(I) and reduced sulfur found in the bulk solution. The overgrowth layer of bornite is not as prominent in this system as the chalcopyrite overgrowth in the replacement of hematite by chalcopyrite (Zhao et al. 2014), but nevertheless the bornite overgrowth does cement grains together.

The reaction extent is temperature and pH dependent and the relative rates are controlled by the dissolution rate of chalcopyrite, which is related to the solubility of chalcopyrite. The equilibrium concentrations of Cu and Fe in the bulk solution under reaction conditions were calculated using HCh, and the results are plotted in Figure 5c. The range in concentrations corresponds to situations where no reaction took place (bornite absent from the system) and situations where the maximum reaction extent

316 was achieved. The minerals assemblages consist of chalcopyrite, optional bornite,
317 chalcocite, and traces of pyrite and covellite. The calculated concentrations of Cu and
318 Fe increase at higher reaction temperature. The predicted concentrations of Fe are
319 very low, especially under basic conditions; Fe solubility decreases at high pH (HS^-
320 main sulfur species in solution), but Cu solubility increases at high pH relative to
321 acidic conditions (H_2S(aq) predominant S species in solution). The calculated Cu
322 solubilities correlate with the reaction extent and the higher Cu concentrations favor
323 the replacement of chalcopyrite by bornite. For example, 85% of chalcopyrite was
324 replaced by bornite in solution CB10 at 320 °C after 24 hr reaction (calculated Cu
325 concentration 4.91×10^{-3} mole•kg^{-1}), while at 200 °C the concentration of Cu in
326 solution CB10 decreased to 1.18×10^{-3} mole•kg^{-1} and no replacement reaction was
327 observed after 24 hr. The effects of Cu concentration on reaction extents was further
328 confirmed by experiments carried out in different buffer solutions at the same reaction
329 temperature. At 250 and 300 °C, the reaction extent increased together with Cu
330 solubility (Fig. 6). Hence, despite the excess Cu in the system, Cu rather than Fe
331 mobility appears to control the dissolution rate of chalcopyrite based on the calculated
332 equilibrium metal concentrations. An alternative explanation is that Fe mobility is
333 controlled by kinetic factors rather than equilibrium. The extremely low predicted Fe
334 solubilities support such a scenario for the transport of excess Fe from the
335 chalcopyrite dissolution front to the bulk solution. In this case, high pH may favor Fe
336 mobility, and Fe may control the dissolution rate of chalcopyrite.

337 **The pathways of mass and solution transport**

338 ICDR reactions are fluid-mediated replacement reactions and the pathways, such as
339 pores, cracks, or grain boundaries in the product phase are essential for fluid and mass
340 transport between the bulk solution and reaction front (Putnis 2009; Jonas et al. 2014).

For most of ICDR reactions with negative volume change, the product is highly porous; for example for the pseudomorphic replacement of calaverite by native gold the volume of the product is reduced to only 21% of the original, based on the preservation of Au (Zhao et al. 2009). In such cases, large amounts of pores are generated in the product to preserve the external volume of the parent phase, and the porosity structure provides the pathway to sustain reaction. Even in some reactions with positive volume change, porosity in the final products provides the pathways for mass transfer (e.g., leucite to analcime; Putnis et al. 2007; Xia et al. 2009b). However, in the transformation of chalcopyrite to bornite, the bornite product is compact, with only a small amount of scattered pores (Figs. 2a and 2b). What is unclear is whether some of the porosity in the product bornite has been destroyed during polishing or healed during the quenching process, but connected porosity or cracks must have been present to enable fluid transport to and from the reaction interface.

The dissolution of a small amount of chalcopyrite greatly increases the concentration of aqueous Fe at the reaction front, but not significantly the concentrations of Cu and S, as these are relatively high in the bulk solutions, and leads to heterogeneous nucleation and subsequently growth of bornite from the boundary solution layer, which is supersaturated with respect to bornite. As the reaction proceeds and the thickness of bornite increases, the large volume expansion associated with reaction (1) is expected to cause a filling of the porosity, and to quickly shut down the reaction.

Instead, the reactions progresses quickly in the first 24 hr, with textures consistent with solute diffusion through a porous layer (Fig. 2a). In some ICDR reactions, reaction progress is allowed by the formation of cracks as a result of the stress

366 associated with the crystallization of the new phase (e.g., ilmenite to rutile, Janssen et
367 al. 2010; serpentinization, Plumper et al. 2012). Although self-generated cracks may
368 have played a role in the replacement of chalcopyrite by digenite, the textures do not
369 support that this is the primary mode of transport in this case. Runs C8 to C16 show
370 that the replacement reaction reaches 77±5% transformation within 24 hr, but then
371 either stalls or progresses slowly, reaching 95±5% after 120 days. Therefore, it is
372 likely that the porosity decayed during the reactions and in effect the reaction became
373 transport-limited in the later stages. Further evidence for a change in transport
374 mechanism in course of the reaction is provided by the raising importance of twin-
375 boundary planes in the control of reaction progress over time (Figs. 2b, 7). Similar to
376 grain boundaries (Jonas et al. 2014), twin planes provide preferential fluid pathways.
377 This mechanism appears to become prominent once porous-fluid flow becomes
378 limited.
379
380 This fast annealing of the porosity in the product bornite could be related to the
381 relatively high mobility of Cu and Fe by solid-state diffusion above 200 °C in *bdss*
382 *(Gruguric et al. 199*. In this temperature interval bornite undergoes two phase
383 transitions: from high to intermediate at 265 °C and from intermediate to low below
384 200 °C (Grguric et al. 1999, 2000). These transformations are associated with Cu and
385 Fe ordering, consistent with high metal mobility. Above 265 °C, bornite (Cu_5FeS_4)
386 and digenite (Cu_9S_5) form a complete solid solution, the bornite-digenite solid
387 solution (*bdss*). The *bdss* structure is based on a cubic close-packed array of S atoms
388 with Cu, Fe and a metal vacancy randomly distributed over all eight available
389 tetrahedral interstices in a “stuffed zinc blende” structure or antifluorite-type structure.
390 Between 200 and 265 °C bornite exists as an intermediate cubic phase, but below

391 200 °C bornite undergoes a complex ordering transition leading to an orthorhombic
392 2*a*4*a*2*a* superstructure (*Pbca*) of the basic zinc blende-type cell (low bornite). The
393 digenite end of the solid solution is characterized by a 5*a* cubic superstructure (*Fm*3*m*)
394 and it appears that a small amount of Fe substituting for Cu stabilizes the
395 superstructure (See Grguric et al. 2000 and references therein). It would only be
396 possible to fully unravel the complex relationship between metal diffusion and
397 porosity, by *in situ* study of the reaction by both diffraction and high resolution
398 tomography techniques.
399

400 **The composition of bornite**

401 The composition of bornite is predominantly temperature dependent, and it becomes
402 Cu-rich and Fe-poor at lower temperature (Figs. 5a and 5b); this corresponds to higher
403 Fe:Cu ratios and a decrease in the digenite component with increasing temperature.
404 The calculated equilibrium concentrations of Cu and Fe in solution both increase at
405 higher reaction temperature, with an increase in Fe:Cu ratio (Fig. 5c); this may
406 contribute to explaining the temperature dependence of the *bdss* composition.
407

408 However, as shown in Figure 5c, the calculated Cu and Fe concentrations are also
409 highly pH dependent. Yet, no significant difference of bornite composition was
410 observed as a function of pH_T. The effect of solution chemistry on the composition of
411 sulfide minerals has been demonstrated in the replacement of pentlandite of violarite
412 by Xia et al. (2008, 2009a). In contrast, solution chemistry appears to play only a
413 minor role on controlling the composition of the *bdss*. Such conclusion is further
414 confirmed by the fact that the bornite compositions are nearly homogeneous. Since
415 the Fe and Cu concentrations in the mother solution are likely to differ at the ICDR

interface and on the outside of the grain, one might expect contrasting compositions to arise in the *bdss* grown from the two different mechanisms. However, the compositions of bornite forming via the replacement of chalcopyrite are essentially the same as those formed from the bulk solution as an overgrowth.

The fact that no compositional variation was observed in bornite may be related to the fast Fe and Cu diffusion within *bdss* at T ≥ 200 ˚C. This was demonstrated by Grguric and Putnis (1999) in their study of rapid exsolution in the *bdss*. The small influence of pH on the composition of the product suggests that the Fe and Cu contents of the fluid do not control the composition of the product in first order. This can be explained if the reaction was buffered by solids, for example:

$$\text{Bornite} = \text{Chalcopyrite} + 2\ \text{Chalcocite};\ K_{P,T} = \frac{a_{chalcopyrite} a^2_{chalcocite}}{a_{bornite}} \quad (5)$$

a_{bornite} represents the activity of the bornite component in the *bdss* solid solution (reaching a value ~1 at 320˚C; Fig. 5a,b). Assuming that chalcopyrite and chalcocite are present and their compositions are close to stoichiometric, $a_{\text{chalcopyrite}} = a_{\text{chalcocite}} = 1$, and

$$a_{\text{Bornite}} = 1/K_{P,T} \quad (6)$$

In this case, the activity of the bornite component depends only on the temperature-dependant stability constant K.

Implications

The textures obtained experimentally for the replacement of chalcopyrite by bornite are strikingly similar to those reported by Halbach et al. (1998) from weathered massive sulfides from Indian Ocean seafloor hydrothermal vents. This work confirms

439 that the replacement of chalcopyrite by bornite proceeds via an ICDR process, with
440 the excess Fe leaving the reaction front and, under the conditions of our experiments,
441 forming an overgrowth of bornite on the outside of the grains, in a manner that is
442 typical of ICDR reactions with large overall volume changes (Zhao et al. 2014).
443 However, the replacement of chalcopyrite by bornite also displays some unique
444 features among ICDR reactions (e.g., Putnis 2009), in particular the chemical
445 homogeneity of the product, the small dependence of the product composition upon
446 solution chemistry, and the lack of prominent porosity. Zhao et al. (2013) showed that
447 complex textures can evolve in simple systems via the interplay of ICDR reactions
448 with diffusion-driven solid-state reactions. We propose that similarly, the unique
449 features of the chalcopyrite to bornite reaction investigated here are related to
450 interaction between a solution controlled ICDR reaction with solid-state diffusion
451 processes. Cationic diffusion in *bdss* is fast relative to the experimental time frame
452 (hours to days) at $T \geq 200$ °C. This fast ionic diffusion can account for the chemical
453 homogeneity of bornite, where inhomogeneity was expected (i.e. differences between
454 bornite formed by ICDR and as overgrowth); and the disappearance of the porosity in
455 the bornite product, possibly leading to the stalling of the reaction after an initial
456 'burst'.
457
458 We also note that there are few stable bornite-digenite solid-solution in nature. One
459 noticeable exception is bornite associated with chalcopyrite in fresh, active sulfide
460 chimney for sea-floor hydrothermal vents (Haymon 1983). The replacement of
461 chalcopyrite by bornite could be used to synthesize bornite of different compositions
462 in order to study the exsolution process of such solid solution.

Acknowledgement

We thank Len Green, Aoife McFadden, and Benjamin Wade from Adelaide Microscopy Center for their assistance in using the FESEM and electron microprobe. We also thank Associate Professor Daniel Harlov and the two referees for their comments and corrections to an earlier version of the manuscript. This work has been made possible by the financial support of the Australian Research Council (Grants DP0880884 and DP1095069). Jing Zhao acknowledges Australian Department of Education, Science and Training, for the International Postgraduate Research Scholarship, and University of Adelaide for the postgraduate scholarship.

References

Akinfiev, N.N. and Zotov, A.V. (2001) Thermodynamic description of chloride, hydrosulfide, and hydroxo complexes of Ag(I), Cu(I), and Au(I) at temperatures of 25-500°C and pressures of 1-2000 bar. Geochemistry International, 39, 990-1006.

Amcoff, Ö. (1988) Experimental replacement of chalcopyrite by bornite: Textural and chemical changes during a solid-state process. Mineralium Deposita, 23(4), 286-292.

Bischoff, J.L. (1991) Densities of liquid and vapors in boiling NaCl-H_2O solutions: a PVTX summary from 300 to 500 °C. American Journal of Science, 291, 309-338.

Brugger, J., Etschmann, B., Liu, W., Testemale, D., Hazemann, J.L., Emerich, H., van Beek, W., and Proux, O. (2007) An XAS study of the structure and thermodynamics of Cu(I) chloride complexes in brines up to high temperature

(400 degrees C, 600 bar). Geochimica et Cosmochimica Acta, 71(20), 4920-4941.

Brugger, J., McFadden, A., Lenehan, C.E., Etschmann, B., Xia, F., Zhao, J., and Pring, A. (2010) A novel route for the synthesis of mesoporous and low-thermal stability materials by coupled dissolution-reprecipitation reactions: mimicking hydrothermal mineral formation. CHIMIA International Journal for Chemistry, 64, 693-698.

Bruker AXS (2009) TOPAS V4.2: General profile and structure analysis software for powder diffraction data. Bruker AXS GmbH, Karlsruhe, Germany

Cook, N.J., Ciobanu, C.L., Danyushevsky, L.V., and Gilbert, S. (2011) Minor and trace elements in bornite and associated Cu-(Fe)-sulfides: A LA-ICP-MS study. Geochimica et Cosmochimica Acta, 75(21), 6473-6496.

Etschmann, B., Liu, W., Testemale, D., Müller, H., Rae, N.A., Proux, O., Hazemann, J.L., and Brugger, J. (2010) An *in situ* XAS study of copper(I) transport as hydrosulfide complexes in hydrothermal solutions (25-592 ˚C, 180-600 bar): Speciation and solubility in vapor and liquid phases. Geochimica et Cosmochimica Acta, 74, 4723-4739.

Graham, U.M., Bluth, G.J., and Ohmoto, H. (1988) Sulfide sulfate chimneys on the East Pacific Rise, 11˚ and 13˚ latitudes. 1. Mineralogy and paragenesis. Canadian Mineralogist, 26, 487-504.

Grguric, B.A. and Putnis, A. (1999) Rapid exsolution behaviour in the bornite-digenite series, and implications for natural ore assemblages. Mineralogical Magazine, 63, 1-14.

509 Grguric, B.A., Harrison, R.J., and Putnis, A. (2000) A revised phase diagram for the
510 bornite-digenite join from in situ neutron diffraction and DSC experiments.
511 Mineralogical Magazine, 64, 213-231.

512 Halbach, P., Blum, N., Münch, U., Plüger, W., Garbe-Schönberg, D., and Zimmer, M.
513 (1998) Formation and decay of a modern massive sulfide deposit in the Indian
514 Ocean. Mineralium Deposita, 33, 302-309.

515 Haymon, R.M. (1983) Growth history of hydrothermal black smoker chimneys.
516 Nature, 301, 695-698.

517 Janssen, A., Putnis, A., Geisler, T., and Putnis, C.V. (2010) The experimental
518 replacement of ilmenite by rutile in HCl solutions. Mineralogical Magazine,
519 74, 633-644.

520 Jonas, L., John, T., King, H.E., Geisler, T., and Putnis, A. (2014) The role of grain
521 boundaries and transient porosity in rocks as fluid pathways for reaction front
522 propagation. Earth and Planetary Science Letters, 386, 64-74.

523 Liu, W. and McPhail, D.C. (2005) Thermodynamic properties of copper chloride
524 complexes and copper transport in magmatic-hydrothermal solutions.
525 Chemical Geology, 221(1-2), 21-39.

526 Mei, Y., Sherman, D., Liu, W., and Brugger, J. (2014) Metal complexation and ion
527 hydration in low density hydrothermal fluids: *ab initio* molecular dynamics
528 simulation of Cu(I) and Au(I) in chloride solutions (25-1000 °C, 1-5000 bar).
529 Geochimica et Cosmochimica Acta, 131, 196–212.

530 Oszczepalski, S. (1999) Origin of the Kupferschiefer polymetallic mineralization in
531 Poland. Mineralium Deposita, 34, 599-613.

Plumper, O., Royne, A., Magraso, A., and Jamtveit, B. (2012) The interface-scale mechanism of reaction-induced fracturing during serpentinization. Geology, 40, 1103-1106.

Putnis, C.V., Geisler, T., Schmid-Beurmann, P., Stephan, T., and Giampaolo, C. (2007) An experimental study of the replacement of leucite by analcime. American Mineralogist, 92, 19-26.

Putnis, A. (2009) Mineral replacement reactions. Reviews in Mineralogy and Geochemistry, 70(1), 87-124.

Qian, G., Brugger, J., Skinner, W.M., Chen, G., and Pring, A. (2010) An experimental study of the mechanism of the replacement of magnetite by pyrite up to 300°C. Geochimica et Cosmochimica Acta, 74(19), 5610-5630.

Qian, G., Xia, F., Brugger, J., Skinner, W.M., Bei, J., Chen, G., and Pring, A. (2011) Replacement of pyrrhotite by pyrite and marcasite under hydrothermal conditions up to 220 °C: An experimental study of reaction textures and mechanisms. American Mineralogist, 96(11-12), 1878-1893.

Qian, G., Brugger, J., Testemale, D., Skinner, W., and Pring, A. (2013) Formation of As(II)-pyrite during experimental replacement of magnetite under hydrothermal conditions. Geochimica et Cosmochimica Acta, 100, 1-10.

Ramdohr, P. (1980) The ore minerals and their intergrowths (2nd edition). Pergamon Press, London.

Robb, L. (2005) Introduction to ore-forming processes. Blackwell Publishing, Oxford.

Roberts, W.M.B. (1963) The low temperature synthesis in aqueous solution of chalcopyrite and bornite. Economic Geology, 58(1), 52-61.

Shvarov, Y. and Bastrakov, E. (1999) HCH: a software package for geochemical modelling. User's guide. AGSO record, 1999/25, 60 pp.

Tenailleau, C., Pring, A., Etschmann, B., Brugger, J., Grguric, B., and Putnis, A. (2006) Transformation of pentlandite to violarite under mild hydrothermal conditions. American Mineralogist, 91, 706-709.

Testemale, D., Brugger, J., Liu, W., Etschmann, B., and Hazemann, J.L. (2009) In-situ X-ray absorption study of iron(II) speciation in brines up to supercritical conditions. Chemical Geology, 264, 295-310.

Tivey, M.K. (1995) The influence of hydrothermal fluid composition and advection rates on black smoker chimney mineralogy - insights from modeling transport and reaction. Geochimica et Cosmochimica Acta, 59, 1933-1949.

Vaughan, D.J. and Craig, J.R. (1978) Mineral chemistry of Metal Sulfides. Cambridge University Press, Cambridge. 493pp.

Xia, F., Zhou, J., Brugger, J., Ngthai, Y., O'Neill, B., Chen, G., and Pring, A. (2008): A novel route to synthesize complex metal sulfides: hydrothermal coupled dissolution-reprecipitation reactions. Chemistry of Materials, 20, 2809-2817.

Xia, F., Brugger, J., Chen, G., Ngothai, Y., O'Neill, B., Putnis, A., and Pring, A. (2009a) Mechanism and kinetics of pseudomorphic mineral replacement reactions: A case study of the replacement of pentlandite by violarite. Geochimica et Cosmochimica Acta, 73(7), 1945-1969.

Xia, F., Brugger, J., Ngothai, Y., O'Neill, B., Chen, G.R., and Pring, A. (2009b) Three-Dimensional Ordered Arrays of Zeolite Nanocrystals with Uniform Size and Orientation by a Pseudomorphic Coupled Dissolution-Reprecipitation Replacement Route. Crystal Growth and Design, 9, 4902-4906.

Zhao, J., Brugger, J., Grundler, P.V., Xia, F., Chen, G., and Pring, A. (2009) Mechanism and Kinetics of a mineral transformation under hydrothermal conditions: calaverite to metallic gold. American Mineralogist, 94, 1541-1555.

582 Zhao, J., Brugger, J., Xia, F., Nogthai, Y., Chen, G. and Pring, A. (2013) Dissolution-
583 reprecipitation vs. solid state diffusion: Mechanism of mineral transformations
584 in sylvanite, $(AuAg)_2Te_4$, under hydrothermal conditions. American
585 Mineralogist, 98, 19-32.
586 Zhao, J., Brugger, J., Ngothai, Y., and Pring, A. (2014) The formation of chalcopyrite
587 and bornite under hydrothermal conditions: an experimental approach.
588 American Mineralogist, 99, 343-354.
589

590 **Figure Captions**

591 **Figure** 1 Secondary electron images of **(a)** unreacted chalcopyrite with sharp edges,
592 **(b)** partially reacted chalcopyrite grains coated with bornite, **(c-d)** the bornite surfaces
593 of partially reacted chalcopyrite grains under hydrothermal conditions, showing
594 bornite crystals varying in size up to 2 μm across.

595 **Figure 2** Back scattered electron images of the cross section of partially reacted
596 grains showing the replacement of chalcopyrite (dark grey, core) by bornite (light
597 grey) after **(a,c)** 1-day (Run No. C11) and **(b,d,e)** 3-day (Run No. C13) reaction at
598 300 ˚C. Inset **(c)** shows reaction initiating on the rim of the chalcopyrite grain and
599 along fractures within the grain. Inset **(d)** shows the sharp boundaries between
600 chalcopyrite and bornite, and fine porosity within the bornite product, and inset
601 **(e)** illustrates the larger pores found within the bornite that formed via overgrowth.

602 **Figure 3** Reaction extents as a function of temperature and pH_T. Experiments were
603 conducted for 24 hrs at 250 ˚C (Run No. C1-C4) and 300 ˚C (C5-C7 and C11) using
604 different fluid compositions. The shade areas in pink show the solution used in the
605 experiments and more details of the solution composition can be found in Table 1.
606 The pH_T values of different fluid compositions at reaction temperature were
607 calculated using HCh and listed in Table 2. Errors of the reaction extent (3-σ; ±5%)
608 are plotted at each point.

609 **Figure 4** XRD patterns of runs at reaction temperatures of 280 ˚C (Run No. T5) and
610 300 ˚C (Run No. T6). The original XRD patterns were shown with blue lines and the
611 refined patterns were shown in red. The grey line at the bottom shows the refinement
612 differences.

Figure 5 The measured Cu:S **(a)** and Fe:S **(b)** molar ratios in the bornite product as a function of reaction temperature, showing that the composition of bornite becomes more Cu-rich and Fe-poor at lower temperature. The Cu:S/Fe:S ratios of bornite and digenite are 1.25/0.25 and 1.8/0, respectively, shown as dashed lines. The pink area is related to bdss. **(c)** Calculated (HCh geochemical model) concentrations of Cu and Fe in bulk solutions as a function of solution pH and temperature for the closed system corresponding to the experimental charges. The range in concentrations shown for each buffer reflects the difference in models including or excluding bornite (i.e., maximum reaction progress versus no reaction). In addition to bornite and chalcopyrite, the predicted mineral associations include chalcocite, and in some cases traces (mostly <1 mol%) of pyrite and covellite.

Figure 6 Reaction extents as a function of the concentration of Cu in bulk solutions at 250 ˚C (Run No. C1-C4) and 300 ˚C (C5-C7 and C11) for different fluid compositions (reaction conditions and solution compositions were listed in Table 1 and Table 2). The concentration of Cu in bulk solutions was calculated using HCh (full charge composition) and listed in Table 3. Errors of the reaction extent (3-σ; ±5%) are plotted at each point.

Figure 7 Schematic diagrams of partly reacted grain showing the reaction pathways in the replacement of chalcopyrite by bornite. Dark blue stands for chalcopyrite (cpy) and light blue for bornite (bn), and the arrows show the direction of bornite growth. Bn-1 forms via replacement of chalcopyrite, and Bn-2 via overgrowth. (a) Initially the reaction front progresses in a homogeneous manner within the chalcopyrite grain, but

637 (b) later on the replacement progresses mainly along cleavage planes of the

638 chalcopyrite.

Tables

Table 1 Composition of buffer solutions

$pH_{25°C}$	Buffer ID	Components					
		Acid	Conc. ($mol•kg^{-1}$)	Base	Conc. ($mol•kg^{-1}$)	Addition	Conc. ($mol•kg^{-1}$)
2.10	CP2	H_3PO_4	0.522	$NaH_2PO_4·2H_2O$	0.477	NaCl	1.007
3.86	CA4	CH_3COOH	0.825	CH_3COONa	0.170	NaCl	1.000
6.90	CP7	$NaH_2PO_4·2H_2O$	0.340	Na_2HPO_4	0.655	NaCl	1.000
9.80	CB10	H_3BO_3	0.533	NaOH	0.449	NaCl	1.000

Table 2 Reaction conditions and results*

No.	T/(°C)	Buffer Solution#	Solution pH_T§	Time (hr)	NaCl ($mol•kg^{-1}$)	Products and weight percentage (%)‡
C1	250	CP2	3.31	24	1	Cpy(97)Bn(3)
C2	250	CA4	4.17	24	1	Cpy(95)Bn(5)
C3	250	CP7	6.09	24	1	Cpy(85)Bn(15)
C4	250	CB10	7.08	24	1	Cpy(84)Bn(16)
C5	300	CP2	3.75	24	1	Cpy(73)Bn(27)
C6	300	CA4	4.39	24	1	Cpy(67)Bn(33)
C7	300	CP7	6.23	24	1	Cpy(28)Bn(72)
C8	300	CB10	7.43	4	1	Cpy(41)Bn(59)
C9	300	CB10	7.43	6	1	Cpy(68)Bn(32)
C10	300	CB10	7.43	18	1	Cpy(54)Bn(46)
C11	300	CB10	7.43	24	1	Cpy(23)Bn(77)
C13	300	CB10	7.43	72	1	Cpy(29)Bn(71)
C14	300	CB10	7.43	96	1	Cpy(39)Bn(61)
C15	300	CB10	7.43	120	1	Cpy(5)Bn(95)
C16	300	CB10	7.43	144	1	Cpy(11)Bn(90)
T1	200	CB10	7.16	192	1	n.d.
T2	220	CB10	7.12	192	1	n.d.
T3	240	CB10	7.13	96	1	n.d.
T4	260	CB10	7.20	48	1	Cpy(28)Bn(72)
T5	280	CB10	7.30	48	1	Cpy(29)Bn(71)
T6	300	CB10	7.43	48	1	Cpy(27)Bn(73)
T7	320	CB10	7.65	24	1	Cpy(15)Bn(85)

* The mass of chalcopyrite, CuCl and thioacetamide are 10 mg, 21.5mg and 0.1890g, respectively. The volume of fluid is 5ml.
# "P" phosphate buffer solution, "A" acetate buffer solutions, and "B" borate buffer solution. For respective compositions refer to Table 1.
§ pH values were calculated at reaction temperature using HCh software.
‡ Obtained from powder X-ray diffraction patterns by Rietveld quantitative phase analysis. "Cpy" stands for chalcopyrite phase and "Bn" for bornite. In some cases two bornite-like phases were refined, the values here are for the sum of the two forms. Error on the phase proportion is estimated to 5% on each determination.
¶ n.d. not determined

645

646 **Table 3 Compositions of products**

No.	T/°C	BF	pH_T*	Metal concentrations in bulk solution# (mol•kg^{-1})		Points§	Composition	Weight percentages of elements in products (wt%) [mean(range)]			*Bdss*‡
				Fe	Cu			Cu	Fe	S	
T7	320	CB10	7.65	3.22E-10	4.91E-3	41	$Cu_{5.16(9)}Fe_{0.86(7)}S_{4.00}$	64.1(63.9-66.2)	9.5(8.6-10.3)	25.2(25.0-25.5)	$Bn_{93}Dg_{7}$
C5	300	CP2	3.75	2.71E-9	3.88E-4	6	$Cu_{5.21(6)}Fe_{0.85(4)}S_{4.00}$	65.7(65.5-65.9)	9.4(9.3-9.6)	25.5(25.2-25.5)	$Bn_{90}Dg_{10}$
C6	300	CA4	4.39	4.94E-9	4.85E-4	15	$Cu_{5.20(9)}Fe_{0.85(5)}S_{4.00}$	65.8(65.1-66.5)	9.3(9.1-10.1)	25.5(25.2-25.9)	$Bn_{91}Dg_{9}$
C7	300	CP7	6.23	2.28E-11	2.48E-3	10	$Cu_{5.38(8)}Fe_{0.89(7)}S_{4.00}$	65.8(65.5-65.8)	9.6(9.4-9.9)	24.7(24.4-25.0)	$Bn_{83}Dg_{17}$
T6	300	CB10	7.43	8.25E-11	4.25E-3	20	$Cu_{5.23(6)}Fe_{0.81(6)}S_{4.00}$	65.5(64.8-65.8)	9.1(8.8-9.7)	25.4(25.1-25.7)	$Bn_{90}Dg_{10}$
T5	280	CB10	7.30	2.13E-11	3.50E-3	33	$Cu_{5.48(9)}Fe_{0.73(9)}S_{4.00}$	67.2(66.0-67.9)	7.9(6.7-8.9)	24.8(24.4-25.5)	$Bn_{78}Dg_{22}$
T4	260	CB10	7.20	5.81E-12	2.82E-3	34	$Cu_{5.81(9)}Fe_{0.60(8)}S_{4.00}$	69.9(68.0-70.9)	6.4(5.5-7.2)	24.3(24.0-24.6)	$Bn_{63}Dg_{37}$
C1	250	CP2	3.31	2.96E-10	3.03E-4	7	$Cu_{6.03(8)}Fe_{0.59(8)}S_{4.00}$	69.6(68.6-70.6)	6.0(7.0-8.5)	23.3(22.4-23.2)	$Bn_{53}Dg_{47}$
C2	250	CA4	4.17	9.06E-11	4.48E-4	4	$Cu_{6.18(9)}Fe_{0.58(5)}S_{4.00}$	70.1(67.4-70.7)	5.9(5.7-5.9)	22.9(22.4-23.3)	$Bn_{46}Dg_{54}$
C4	250	CB10	7.16	3.16E-12	2.51E-3	8	$Cu_{6.30(7)}Fe_{0.50(6)}S_{4.00}$	70.8(70.4-71.2)	4.9(4.6-5.0)	22.7(22.4-22.9)	$Bn_{41}Dg_{59}$
T3	240	CB10	7.13	1.77E-12	2.21E-3	29	$Cu_{6.04(7)}Fe_{0.45(9)}S_{4.00}$	71.7(69.3-72.4)	4.3(3.5-7.0)	23.9(22.4-24.4)	$Bn_{53}Dg_{47}$
T1	200	CB10	7.16	2.49E-13	1.18E-3	40	$Cu_{6.17(9)}Fe_{0.33(4)}S_{4.00}$	72.7(71.9-73.5)	3.5(3.9-3.1)	23.8(23.4-24.3)	$Bn_{47}Dg_{53}$

* pH values were calculated at reaction temperature using HCh software.
# The concentrations of copper and iron in the bulk solution were calculated using HCh under reaction conditions.
§ The numbers of microprobe analysis points
‡ *"bdss"* refers to bornite-digenite solid solution and the compositions were denoted by Bn_xDg_{100-x}, in which x means the percentage of bornite in the *bdss*; x is calculated on the basis of the Cu content following the equation $x=(7.2-s_{Cu})/2.2*100$, where s_{Cu} is the stoichiometric coefficient of Cu on a 4-sulfur basis (see composition column).

647

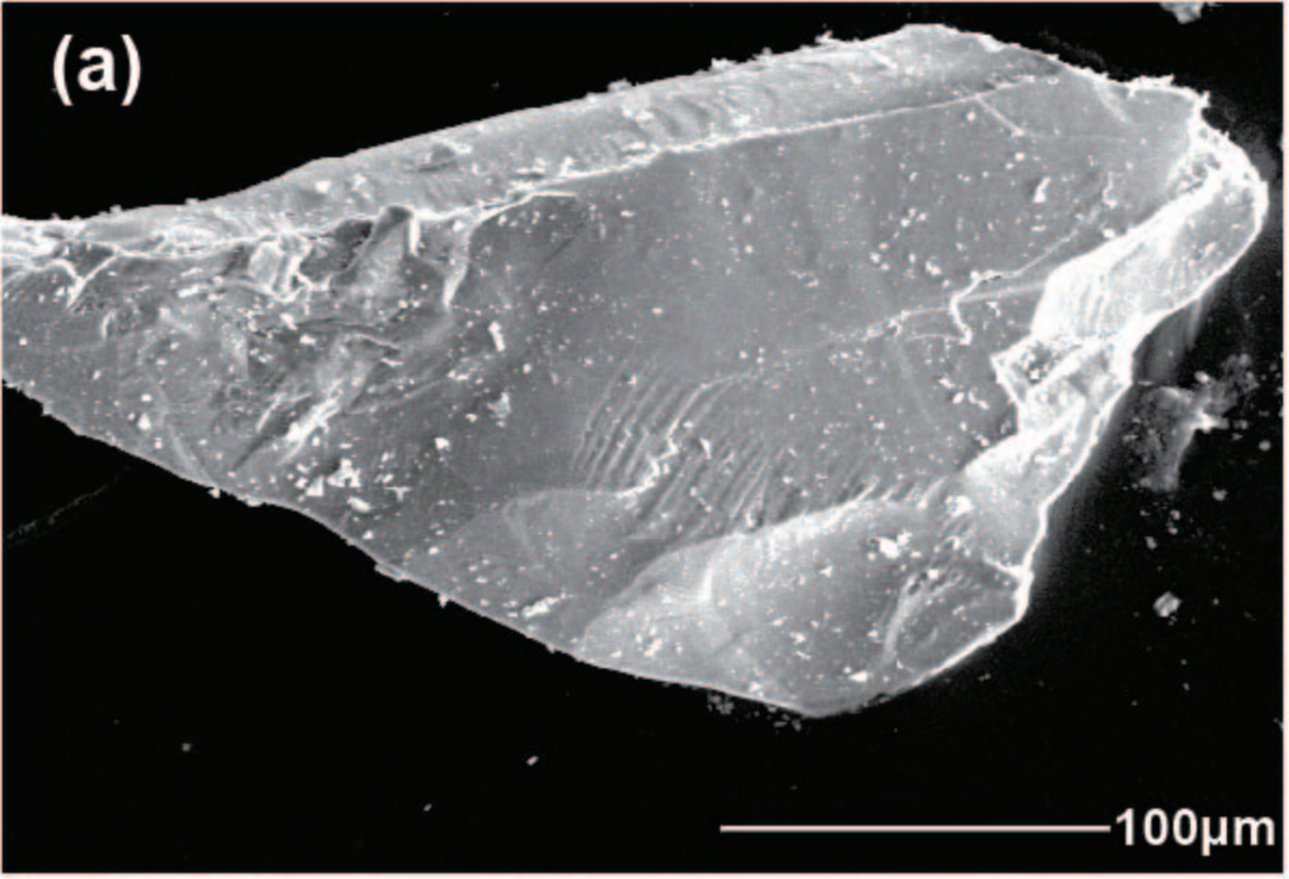
(a)
100μm

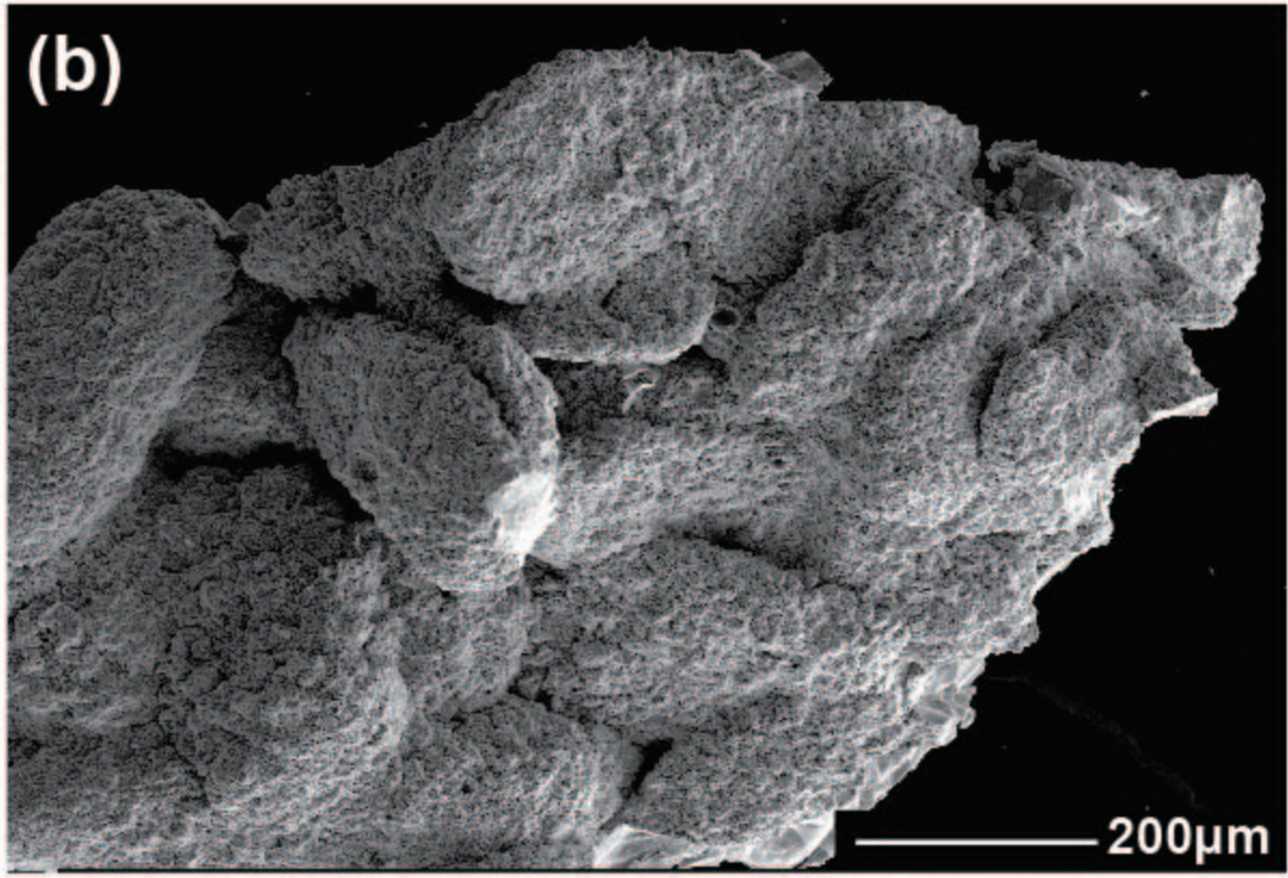
(b)
200μm

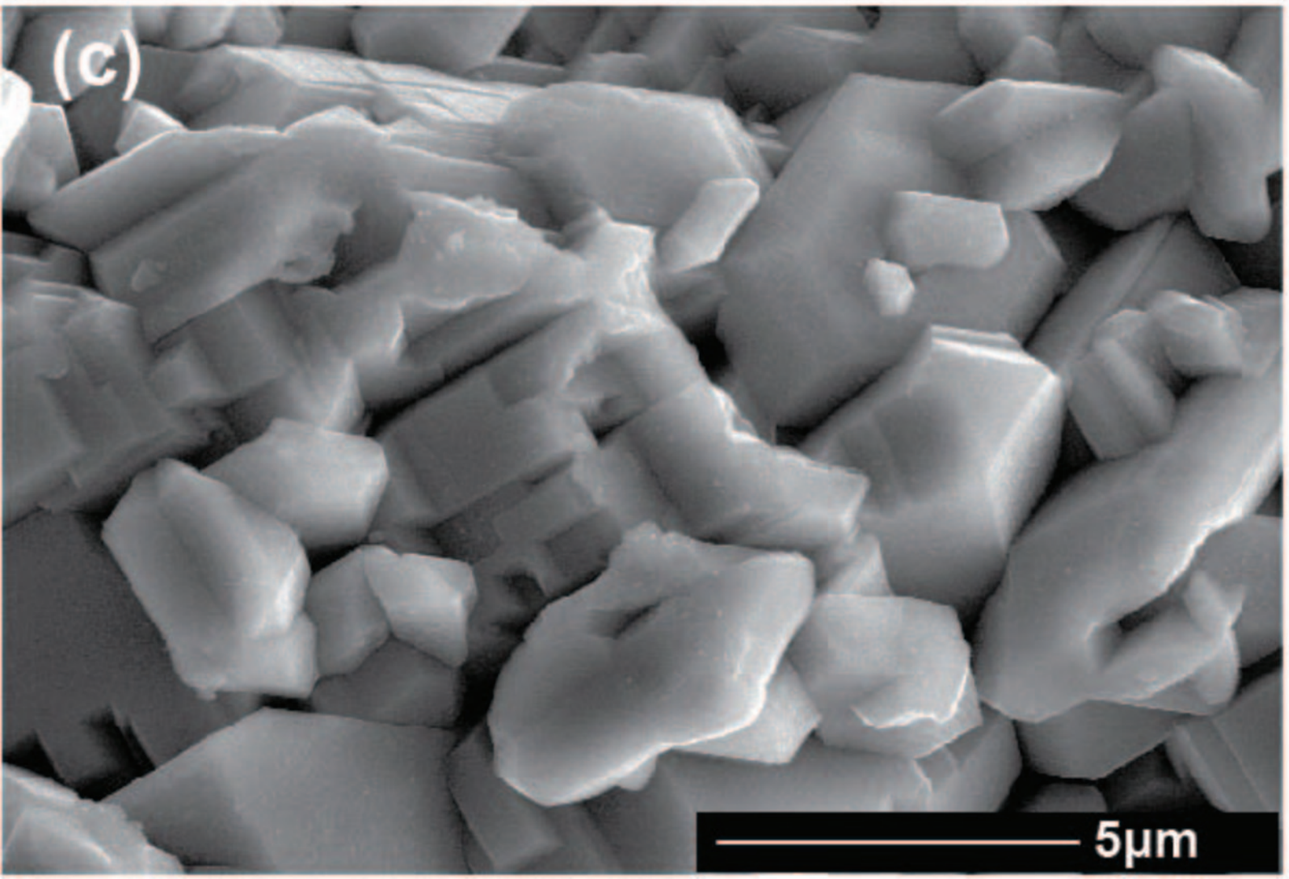
(c)
5μm

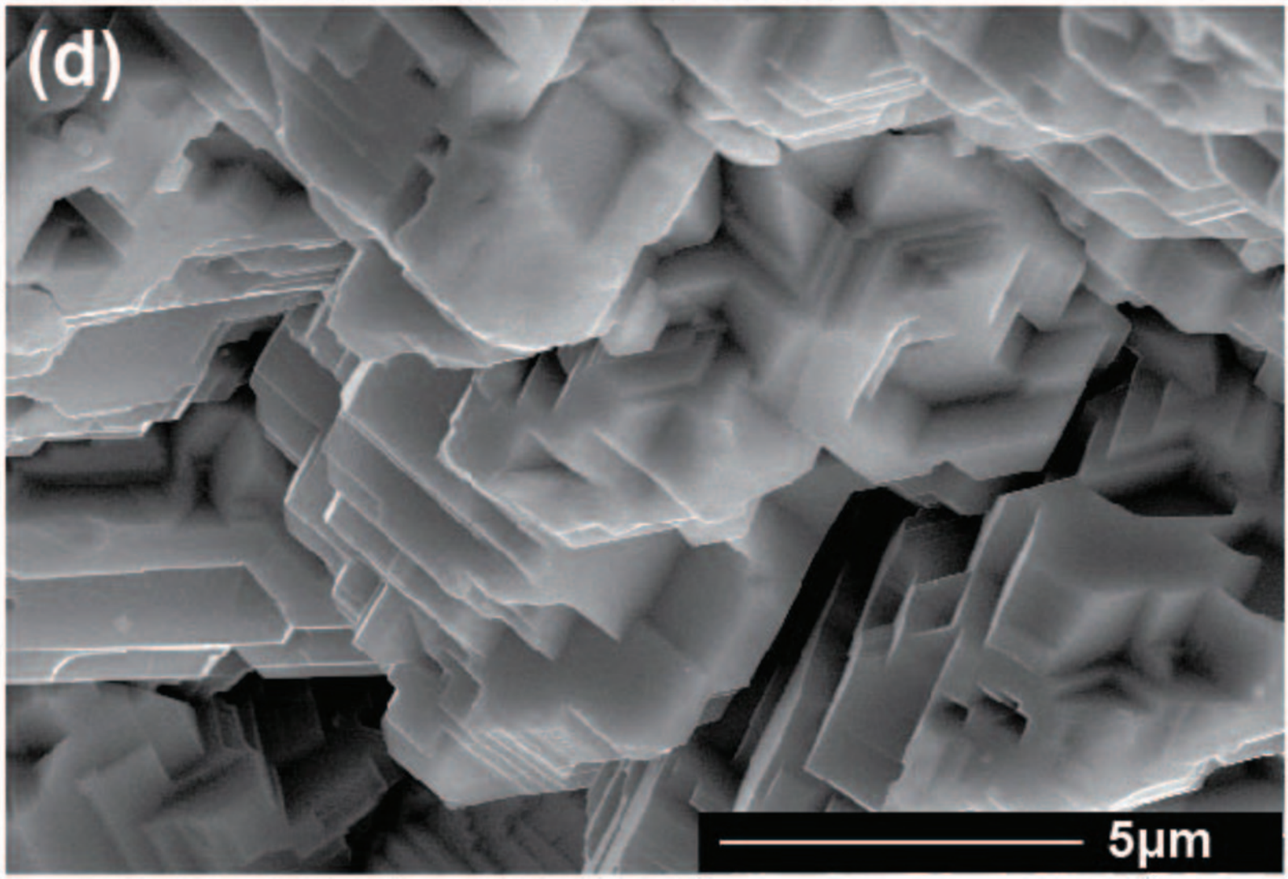
(d)
5μm

(a)

(c)

Bn

CPY

20μm

Bn

CPY

CPY

50μm

(b)

Bn

(d)

CPY

Bn

5μm

CPY

Bn

100μm

(e)

Bn

20μm

250 300

CP2 CA4 CP7 CB10

Reaction Extent / %

100 90 80 70 60 50 40 30 20 10 0

1 2 3 4 6 7 8 11

3.0 3.5 4.0 4.5 5.0 5.5 6.0 6.5 7.0 7.5

pH

T6

Chalcopyrite 27.16 %

Bornite 72.84 %

T5

Chalcopyrite 28.57 %

Bornite 71.43 %

4,000
3,000
2,000
1,000
0
-1,000

3,000
2,000
1,000
0
-1,000

25 30 35 40 45 50 55 60 65 70 75 80

(a)

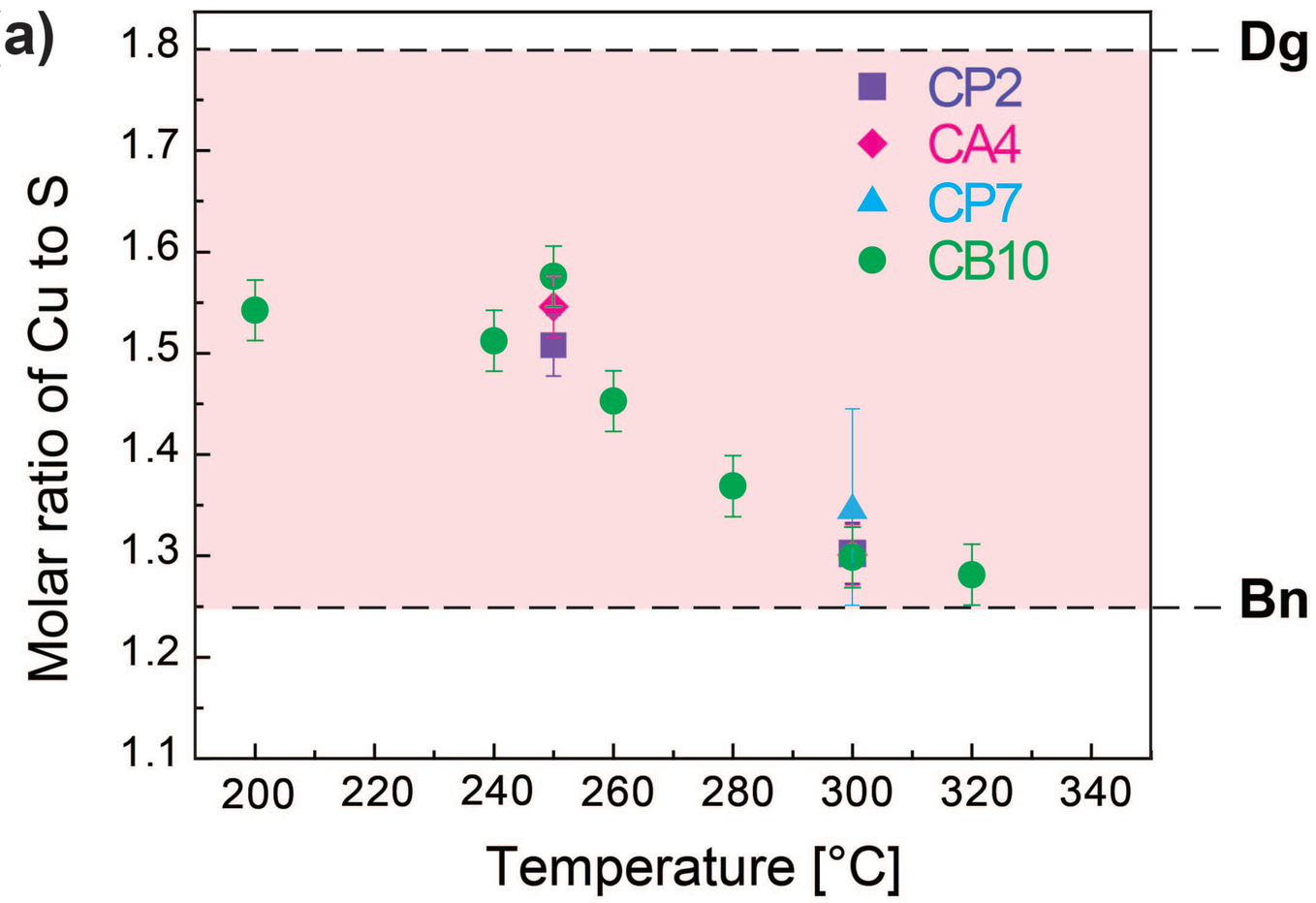
Molar ratio of Cu to S
1.8
1.7
1.6
1.5
1.4
1.3
1.2
1.1
200
220
240
260
280
300
320
340
Temperature [°C]
Dg
Bn
CP2
CA4
CP7
CB10

(b)

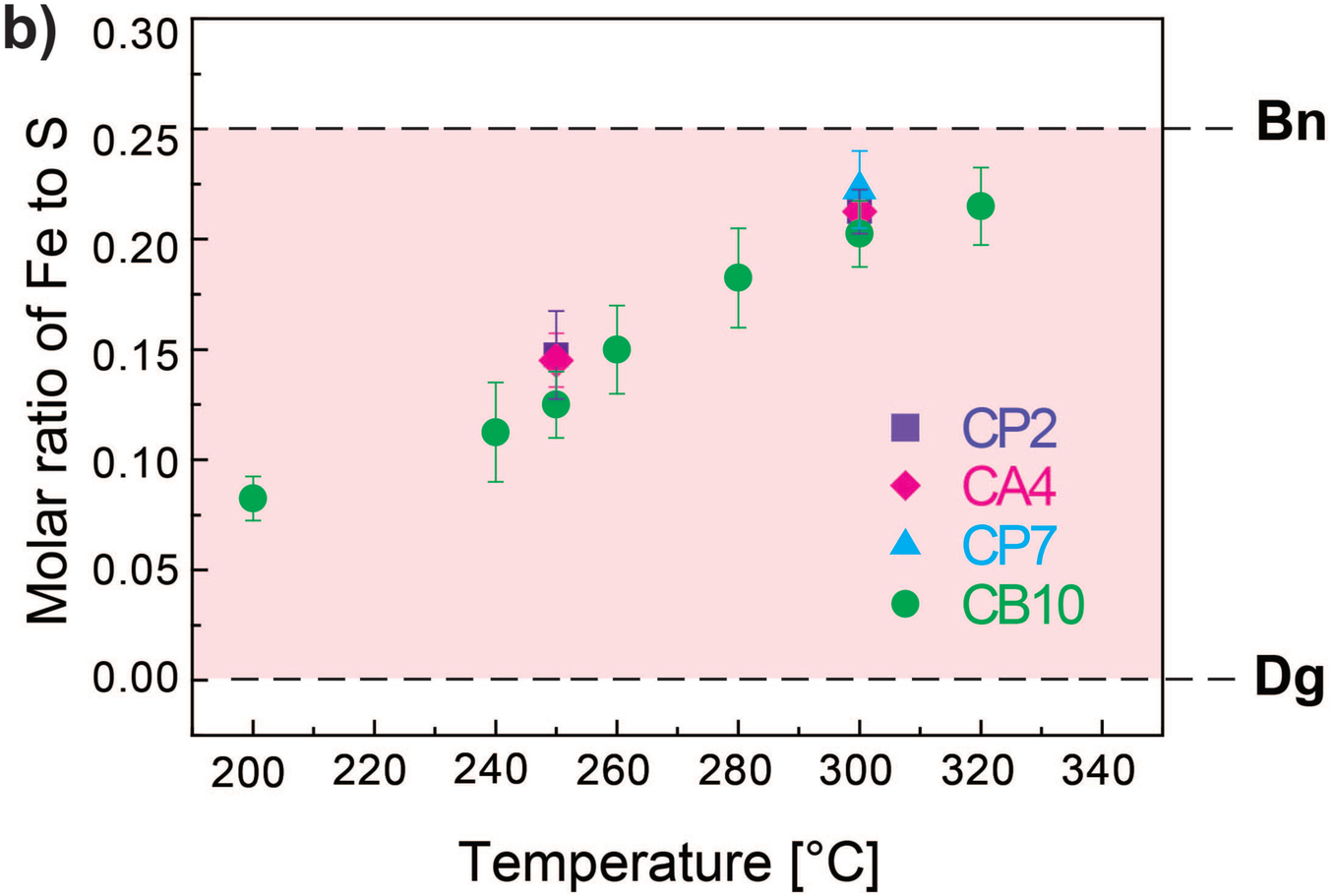
Molar ratio of Fe to S
0.30
0.25
0.20
0.15
0.10
0.05
0.00
200
220
240
260
280
300
320
340
Temperature [°C]
Bn
Dg
CP2
CA4
CP7
CB10

(c)

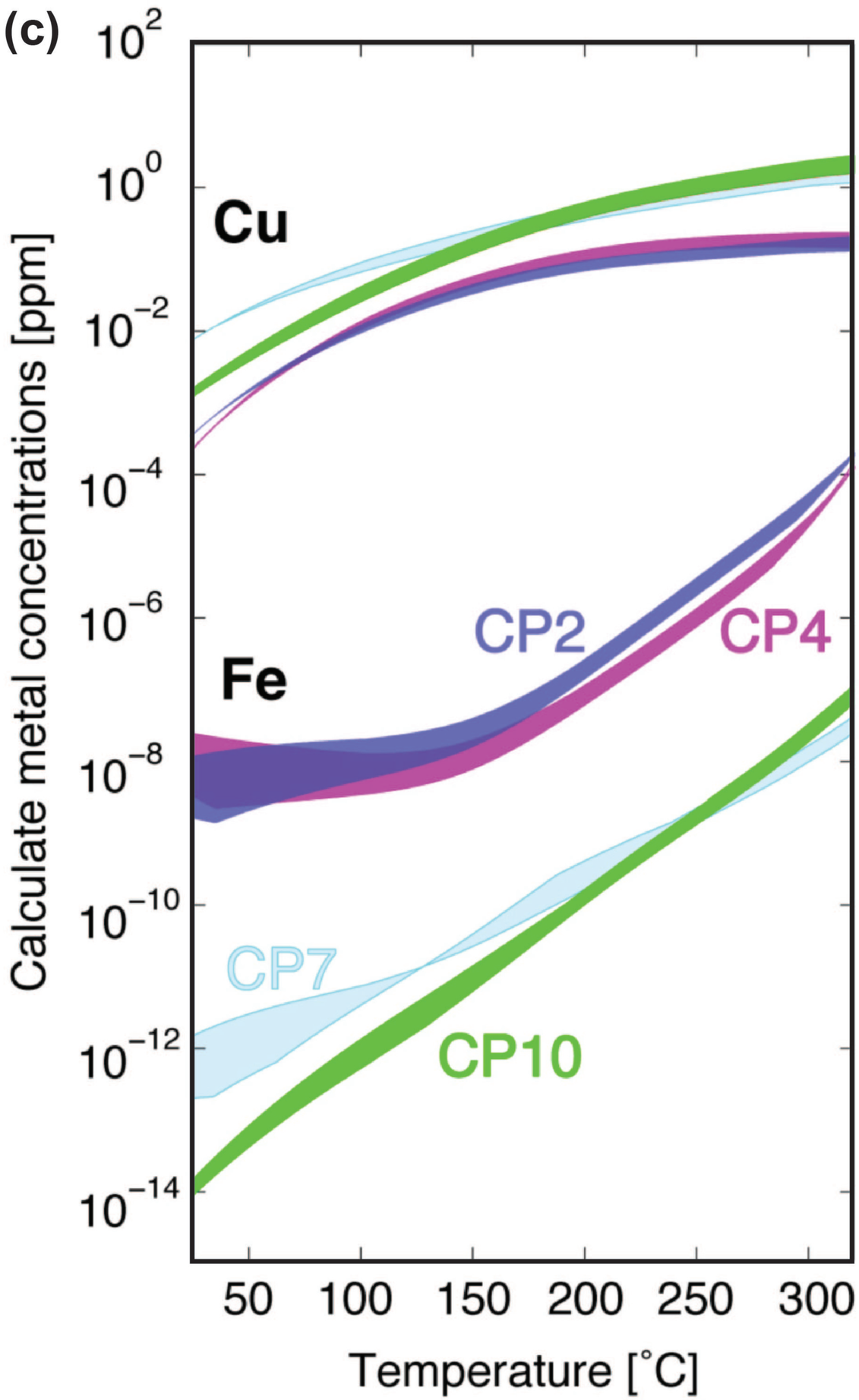
Calculate metal concentrations [ppm]
10^{2}
10^{0}
10^{-2}
10^{-4}
10^{-6}
10^{-8}
10^{-10}
10^{-12}
10^{-14}
Cu
Fe
CP2
CP4
CP7
CP10
50
100
150
200
250
300
Temperature [°C]

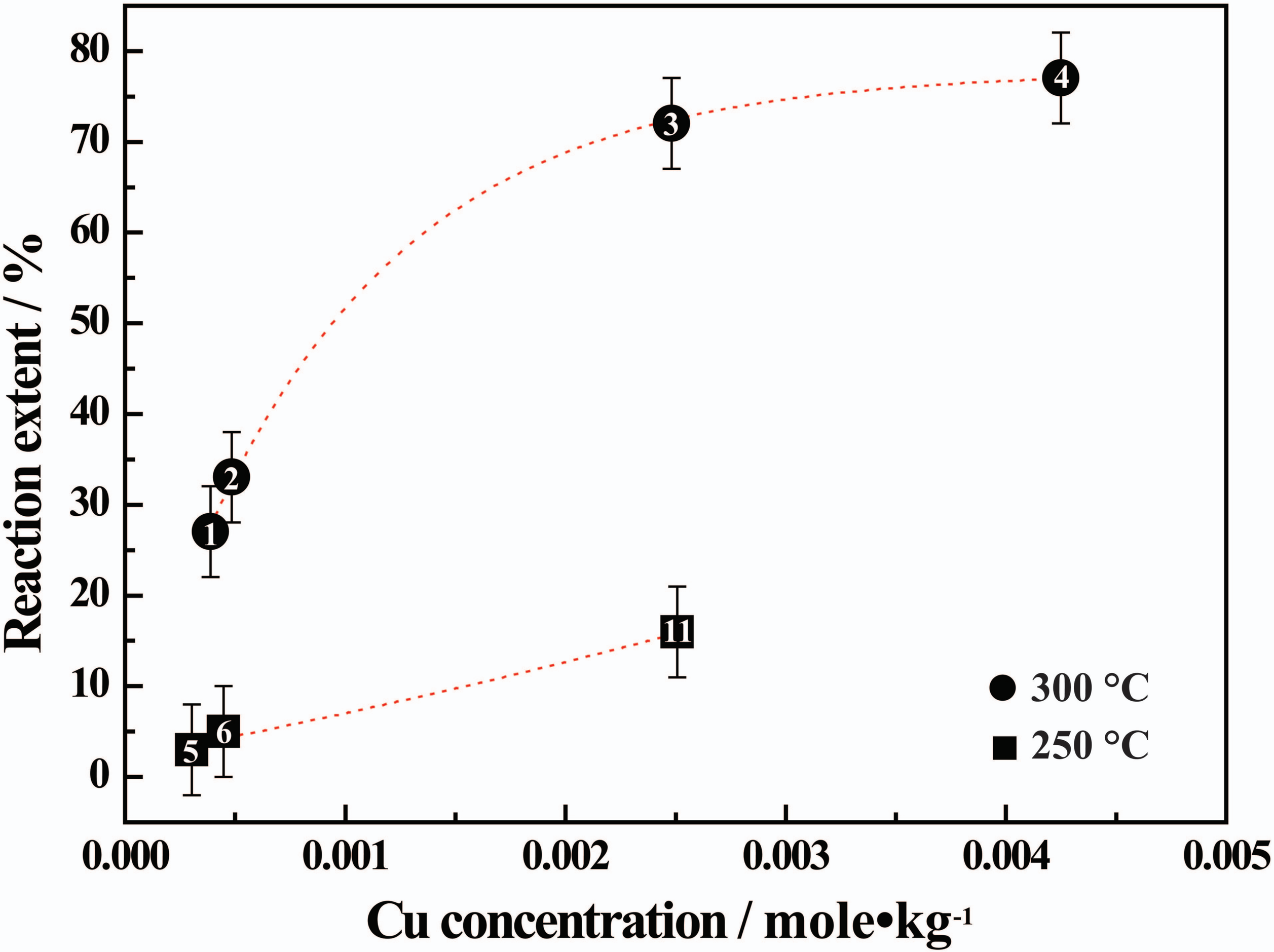
Reaction extent / %
80
70
60
50
40
30
20
10
0
0.000
0.001
0.002
0.003
0.004
0.005
Cu concentration / mole•kg-1
1
2
3
4
5
6
11
300 °C
250 °C

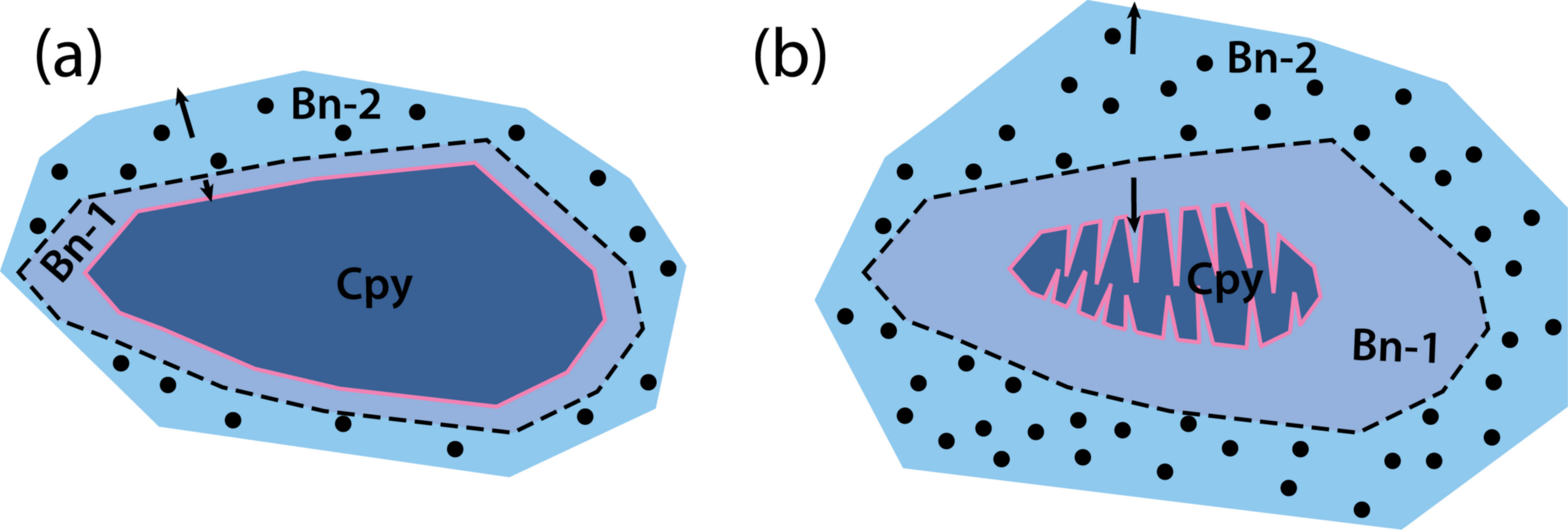
(a)
Bn-2
Bn-1
Cpy
(b)
Bn-2
Cpy
Bn-1